Fragmentation and Limits to Dynamical Scaling in Viscous Coarsening: An Interrupted *in situ* X-Ray Tomographic Study

David Bouttes,[1,*] Emmanuelle Gouillart,[2] Elodie Boller,[3] Davy Dalmas,[2] and Damien Vandembroucq[1]
[1]*Laboratoire PMMH, UMR 7636 CNRS/ESPCI/University Paris 6 UPMC/University Paris 7 Diderot, 10 rue Vauquelin, 75231 Paris Cedex 05, France*
[2]*Surface du Verre et Interfaces, UMR 125 CNRS/Saint-Gobain, 93303 Aubervilliers, France*
[3]*European Synchrotron Radiation Facility (ESRF), BP 220, 38043 Grenoble, France*
(Received 16 September 2013; published 18 June 2014)

X-ray microtomography was used to follow the coarsening of the structure of a ternary silicate glass experiencing phase separation in the liquid state. The volumes, surfaces, mean, and Gaussian curvatures of the domains of minority phase were measured after reconstruction of the 3D images and segmentation. A linear growth law of the characteristic length scale $\ell \sim t$ was observed. A detailed morphological study was performed. While dynamical scaling holds for most of the geometrical observables under study, a progressive departure from scaling invariance of the distributions of local curvatures was evidenced. The latter results from a gradual fragmentation of the structure in the less viscous phase that also leads to a power-law size distribution of isolated domains.

DOI: 10.1103/PhysRevLett.112.245701 PACS numbers: 64.75.-g, 47.51.+a, 61.43.Fs, 81.70.Tx

Introduction.—The construction of a theoretical framework describing the phase separation of binary liquids [1–3] has been fueled by successive experimental developments. Up until the 1990s, most experimental observations were performed in the Fourier space, with light or neutron scattering. Model systems were immiscible solutions [4,5], polymer blends [6,7], or glasses [8]. These experiments confirmed that the dynamical scaling assumption is relevant for these systems; i.e., it is possible to rescale the structure factor by a unique length scale ℓ. This length increases with a power law: $\ell(t) \sim t^{\alpha}$, α depending on the growth regime [9]. More recent numerical simulations confirmed this scaling behavior and provided some insights about the geometry in real space [10–12]. Meanwhile, access to direct space was made possible by new techniques of observation, such as scanning laser confocal microscopy: curvatures could be measured on phase-separated polymer blends [13,14]. These observations are especially relevant to discuss the local mechanisms that govern the coarsening; for instance, pinch-off was observed in a colloidal glass [15]. Recent predictions concerning statistical quantities such as size or surface distributions of domains [16,17] as well as numerical studies of aging in phase-separating fluids [18,19] also motivate the observation in real space.

The effect of dynamical asymmetry (diffusivity, viscosity) on the morphology has recently raised a growing interest. Experiments on polymers revealed the spectacular influence of viscoelasticity [20]. Recent work [21] evidenced a logarithmic (stress-assisted) growth for a gas-glass phase separation. Numerical simulations with a viscosity contrast [22,23] showed a strong effect on morphology. However, the influence of a sole viscosity contrast has not yet been experimentally investigated in the hydrodynamical regime.

The development of x-ray microtomography provides a suitable tool to explore phase separation in three dimensions, with submicron spatial resolution reached in synchrotron facilities [24,25]. Phase-separated polymer blends were already observed with phase-contrast imaging [26].

Glass-forming liquids offer an interesting opportunity to study phase separation [8]. A fast quench below the glass transition temperature enables one to study the frozen structure in the solid state, thereby extending the variety of available characterization techniques. Transmission and scanning electron microscopy, Raman scattering, and atomic force microscopy have been used to quantitatively characterize phase separation in glasses [27–29]. We focus here on the late stage of spinodal decomposition after a deep quench into the unstable region, which produces interconnected structures. After an initial stage where the interfaces form, the growth can be described by a competition between the interfacial tension, which favors the decrease of the surface area between each phase, and dissipative forces (e.g., viscosity and inertia).

In the following, we first present results on the observation of the coarsening in silicate melts at high temperatures, using x-ray microtomography. After a description of the experimental system, a 3D analysis of the main features of the coarsening stage is given. The dynamical scaling hypothesis is tested up to its limits on a full set of morphological observables. Associated with the onset of a fragmentation process, a gradual departure from scaling invariance is observed on local curvatures.

Materials and methods.—A model glass for phase separation: Using the knowledge available in glass science

[8], we designed a barium borosilicate glass to study phase separation. The composition of the glass was 57.1 wt% SiO_2, 23.3 wt % BaO, 18.9 wt % B_2O_3. Elaborated from raw materials, this composition was subsequently checked by wet chemical analysis. The glass decomposes into two phases: a minority barium-rich phase, and a majority barium-poor phase. This ensures a good absorption contrast for x-ray tomography, as barium is much more absorbent than the other elements. This system has a large metastable region that extends well above the liquidus [30,31], which is appropriate to study the coarsening of a binary liquid. The viscosity contrast in the range of temperatures of our experiments is very high, the minority phase being much less viscous than the majority phase.

After elaboration, an interconnected microstructure of typical size ≈ 1 μm was already present because of the large temperature difference between the decomposition dome and the glass transition temperature, which permitted phase separation even during a fast quench.

X-ray tomography: A series of microtomography experiments were performed on the ID19 beam line at the European Synchrotron Radiation Facility (ESRF). Samples 2 mm in diameter were placed into refractory crucibles, and the glass samples were then observed during a heat treatment at a temperature corresponding to a liquid state. Three experiments were done at different temperatures, 1080°C, 1130°C, and 1180°C, using an interrupted *in situ* protocol [25]. The samples were quenched in air at regular time intervals to room temperature. They were subsequently scanned, then heated again to the working temperature until the next quench. The typical time scale for the temperature changes is of the order of a few seconds. Because of the glassy nature of the material and the relatively fast quench, compared to the characteristic time of the domain growth, it is expected that the successive quenches should not influence the main features of the coarsening. We used a pink beam x-ray radiation with a peak photon energy at 31 keV. For each scan, 900 x-ray radiographies were recorded, from which the 3D absorption field was reconstructed using the standard filtered-back projection algorithm, resulting in volumes of $512 \times 1024 \times 1024$ pixels. Pixel size was 0.7 μm and scan time was approximately 5 min.

Image processing: In order to study the geometrical and temporal evolution of each phase during demixing, the following image processing was used. First, reconstructed 3D images were denoised using a total variation filter [32]; the barium-rich and silica-rich phases were subsequently identified with a random walker algorithm [33] (see Supplemental Material [34]). The different domains could then be identified as distinct connected components. Then, geometrical characteristics, such as volume V_i, surface S_i of all domains i, and local curvatures, were computed from the statistics of neighboring configurations of eight-voxel cubes [35,36]. Curvatures were obtained from a local fit of the interface by a quadric [37].

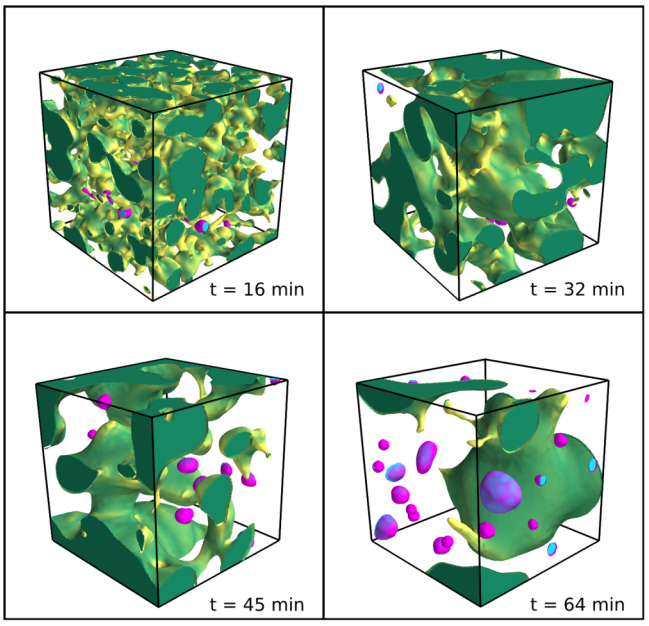

FIG. 1 (color online). 3D visualization [38] of the barium-rich phase, from scans after different times at 1130°C (16, 32, 45, and 64 min). The brightness contrast represents the absolute value of the mean curvature (shades of green for the percolating domain, shades of purple for the isolated domains). The lateral size of the cube is 140 μm. The coarsening of the structure is accompanied by a fragmentation of the spanning cluster into isolated domains.

Results.—After reconstruction and segmentation, the visual observation of a time series of images (Fig. 1) offers an intuitive idea of the coarsening. Most of the minority phase (barium rich), the volume fraction of which is $35 \pm 5\%$, lies in a percolating network, but we also observe a growing fraction of isolated domains when time increases. The coarsening appears clearly: the width of the domains grows, and their surface gets smoother and smoother.

In the following, we first study quantities averaged over the whole volume, in analogy to previous experiments, to show the linear growth in time of the typical scale. Then, we give a more detailed account of the morphological features of the interconnected structure and their time evolution. Finally, we characterize the development of a growing fraction of isolated domains.

Viscous coarsening: As mentioned before, various coarsening regimes have been proposed for phase separation, depending on the leading driving forces (diffusion, viscosity, inertia, etc.). The general scaling law is $\ell \sim t^{\alpha}$. Here, we define ℓ, the characteristic length scale, as 3 times the ratio between the total volume V_{tot} and the total surface area S_{tot} of the minority phase,

$$\ell = 3(V_{\mathrm{tot}}/S_{\mathrm{tot}}). \quad (1)$$

The prefactor 3 is chosen so that the characteristic length of a system of spheres of radius $r = \ell$ is exactly ℓ.

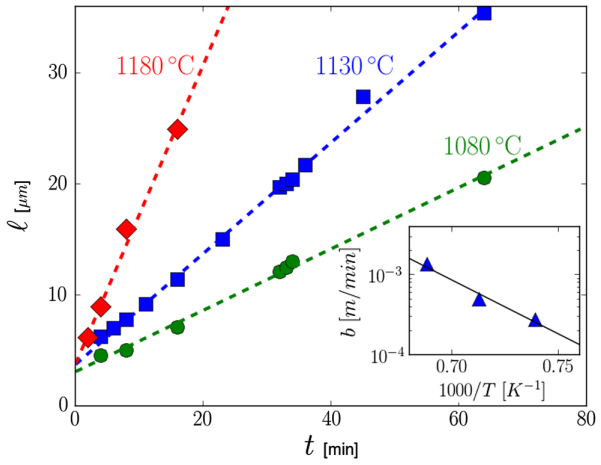

FIG. 2 (color online). Characteristic length ℓ vs time t, for temperatures 1080°C (filled circle), 1130°C (filled square), and 1180°C (filled diamond). The dotted lines are linear fits. Inset: semi-log plot of the slopes of the linear fits b, as a function of the inverse temperature $1/T$.

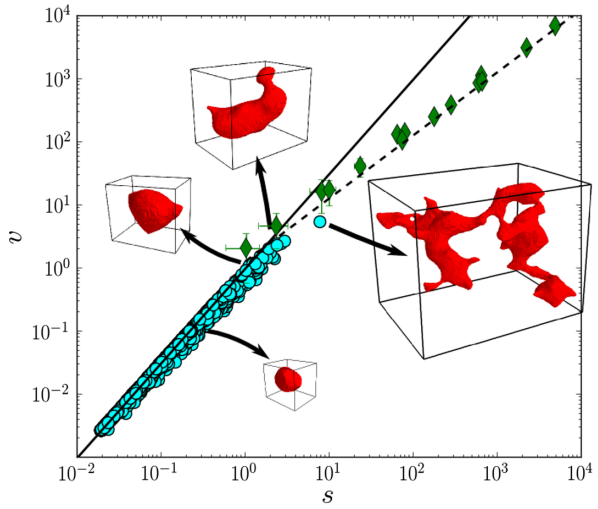

FIG. 3 (color online). Rescaled volumes v of the domains vs their rescaled surfaces s, for all isolated domains (filled circle) and for the percolating domain (filled diamond) after 16, 32, 45, and 64 min at 1130°C. The error bars indicate the standard deviation of the measures for all boxes of a given size. The black solid line is $v = s^{3/2}$ (ideal spheres), and the black dotted line is $v \sim s$. Some domains shapes are shown as examples.

The time evolution of this length is plotted on Fig. 2 for $T = 1080$°C, 1130°C, and 1180°C, along with linear fits. As there was already a microstructure at the beginning of the experiment, $\ell(t = 0) \neq 0$. Our results are consistent with the linear growth proposed by Siggia [39] due to a hydrodynamic flow controlled by a competition between surface tension γ and viscosity μ,

$$\ell(t) \sim (\gamma/\mu)t. \tag{2}$$

This mechanism assumes that the Laplace pressure due to local curvatures induces a flow. It requires the minority phase to be interconnected, because the flow inside isolated domains stops as the isolated domains approach a sphere. During the experiment, most of the minority phase remains in the percolating domain (final volume ratio of about 75% to 90% in our experiments), so we do not expect a significant slowing-down on the measure of ℓ. The coarsening is faster at higher temperature, due to the decrease of viscosity. Growth rates at different temperatures seem consistent with an Arrhenius law (Fig. 2, inset).

Domain shape: Using the data from individual domains, we characterize their shape from the relation between their surface area and their volume. In order to characterize the shapes at different times, we normalize the volume V and the surface S of each domain, using the characteristic length scale ℓ,

$$v = V/[(4/3)\pi\ell^3]; \qquad s = S/(4\pi\ell^2). \tag{3}$$

The reduced volume v is plotted as a function of the reduced volume s for all domains and different times in Fig. 3. When close to a sphere, the volume of a domain should lie close to the solid line representing the sphere case. If more elongated, or ramified (see examples of domains in Fig. 3), it should have an excess of surface compared to a sphere, and hence move away from this line. According to this classification, we observe that most of the small domains are close to a spherical shape, whereas bigger domains deviate more and more as their volume increases. The dynamic length scale $\ell(t)$ separates a dominant population of small spheroidal clusters from a lower fraction of large ramified clusters.

Despite poor statistics on large domains, a natural assumption would be to consider that the shape of large domains is inherited from the percolating structure, as isolated domains detached from it. They would subsequently change their shape towards spheres and/or fragment into additional smaller domains. If we plot the normalized volume of the percolating domain v_p as a function of its rescaled surface s_p, measured at different times and in boxes of different sizes within a given image, we find a linear relation: $v_p \sim s_p$, see Fig. 3, dotted line. The large ramified domain shape also follows the same linear relation, and the crossover between the large and small domains corresponds well to the intersection of the two asymptotic regimes. Note that a nontrivial exponent could have been expected, with an initial condition closer to the percolation threshold in three dimensions [16,17].

Local curvatures: Another benefit of real-space imaging is the possibility to access local geometrical observables, such as local curvatures [14,40] of the minority phase. In Fig. 4(a) we show the distributions of the Gaussian curvature K obtained after 16, 23, 32, 45, and 64 min at 1130°C. As expected, the distribution becomes narrower and narrower along the coarsening process. The asymmetry

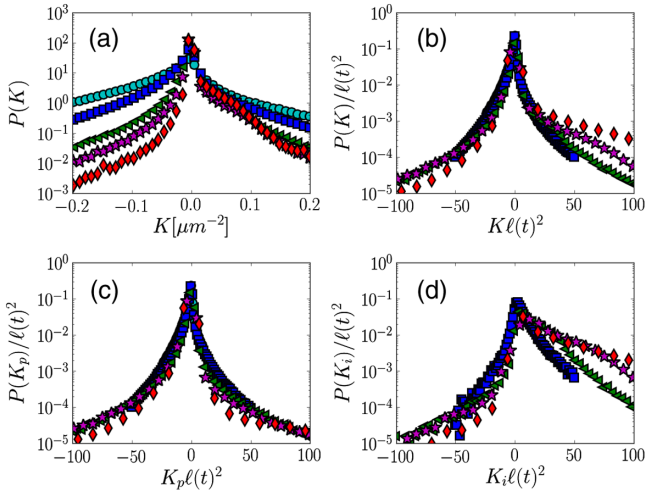

FIG. 4 (color online). Gaussian curvature distributions K, K_p, and K_i, before (a) and after rescaling for all domains (b), only percolating (c), and only isolated domains (d), after 8 (filled circle), 16 (filled square), 32 (filled triangle), 45 (filled star), and 64 min (filled diamond) at 1130°C.

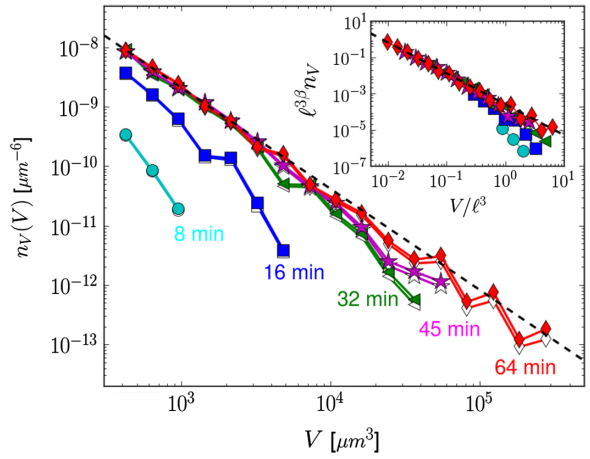

FIG. 5 (color online). Domain volume distribution $n_v(V)$ (except percolating domain) after thermal treatment at $T = 1130$°C during 8, 16, 32, 45, and 64 min. The dotted line is $n_V \sim V^{-\beta}$, with $\beta = 1.7$. The open symbols show the size distributions before the correction due to the finite size of the field of view. The inset shows the same results after rescaling by the dynamical length $\ell(t)$.

of Gaussian curvatures reflects the topology of the structure, the surface being dominated by saddlelike shapes (negative value). For the whole system, the time evolution appears to be reasonably well captured by means of a simple rescaling by the dynamic length,

$$P(K) = \ell^2 \Psi[K\ell(t)^2].$$

After rescaling [see Fig. 4(b)], the distribution collapses onto a master curve (Ψ); a similar collapse is observed for the mean curvature (see Supplemental Material [34]). Still, this collapse is limited by the fragmentation of the percolating domain. An additional positive Gaussian curvature appears with time due to the increasing number of isolated domains. Real-space imaging therefore enables us to show the origin of this gradual departure from scaling invariance. When restricted to the percolating cluster [K_p, Fig. 4(c)], a perfect collapse is recovered, while a clear breaking of scaling invariance is obtained when the same analysis is performed within the subset of isolated domains [K_i, Fig. 4(d)]. The collapse indicates that any measure of ℓ would be equivalent (which was checked by, e.g., using chord length distribution, or the spatial correlation function). In addition, because only the percolating domain has a self-similar growth, one should prefer a measure of ℓ that excludes other domains; here, their contribution is limited by their small volume fraction.

Fragmentation: As was shown previously in Fig. 1, isolated domains are not observed in the early stage of the experiment, but they grow in number during the experiment, as a consequence of a fragmentation of the initial percolating structure. We show in Fig. 5 the time evolution of size distribution of the domains per unit volume n_V, computed as the probability density to find a domain of volume V per unit volume, measured at 1130°C. Very small domains of linear size smaller than ten pixels are hard to identify with certainty, and are therefore not shown here. We computed the sampling bias affecting large domains that touch the boundaries of the field of view (see Supplemental Material [34]). We observe that more domains are present at longer times. In addition, the tail of the distribution changes with time, since large domains are observed at longer times. Despite the difficulty to obtain robust statistics for these large domains, the distribution seems to converge towards a power law distribution: $n_V \sim V^{-\beta}$ with an exponent $\beta \approx 1.7 \pm 0.1$.

The power-law distribution seems to develop due to the formation of larger domains that detach from the percolating domain after some time, while the distribution of small domains remains fairly constant once they are formed. This suggests that an intrinsic size distribution exists and can be rescaled by $\ell(t)$. The difficulty to sample very small domains would hide the power-law behavior for these domains at early times. Therefore, we tested the scaling [with $\ell(t)^3$ as characteristic volume]

$$n_V(V) \sim \ell^{-3\beta} \Phi[V/\ell^3], \tag{4}$$

and obtained a reasonable collapse of the data as illustrated in Fig. 5 for the experiment performed at 1130°C.

With the assumptions that domains of volume V detach at time $t \propto \ell(t) = V^{1/3}$, and that a larger number N_{break} of breaking events occur in a more ramified domain according to $N_{\text{break}} \sim \ell^{-3}$, we obtain the distribution of domain volumes $n_V = N_{\text{break}}(dt/dV) \sim V^{-5/3}$, consistent with our observation $\beta \simeq 1.7$.

Conclusion.—The use of interrupted *in situ* x-ray tomography gives access to a full 3D characterization of the coarsening process. Dynamic scaling was shown to account well for the evolution of all geometrical observables. However, a detailed morphological analysis, including the measurements of local curvatures, allowed us to observe a progressive departure from scaling invariance. The latter results from the gradual fragmentation of the (minority) interconnected domain. This process induces a complex multiscale microstructure, with a power-law distribution of isolated domain volumes, that coexists with the percolating phase.

This work was supported by the ANR program "EDDAM" (ANR-11-BS09-027). Experiments were performed on beam line ID19 at the ESRF in the framework of proposal HD501. We gratefully acknowledge the help of J. Grynberg, A. Lelarge, S. Patinet, F. Lechenault, and J.-P. Valade for performing the experiments at the ESRF, as well as fruitful conversations with M.-H. Chopinet and L. Cugliandolo. We thank Yohann Bale for his help in sample preparation and Erick Lamotte for the glass elaboration.

*david.bouttes@espci.fr

[1] A. J. Bray, Adv. Phys. **43**, 357 (1994).
[2] A. Onuki, *Phase Transition Dynamics* (Cambridge University Press, Cambridge, England, 2002).
[3] R. W. Ballufi, S. M. Allen, and W. C. Carter, *Kinetics of Materials* (Wiley Interscience New York, 2005).
[4] Y. Chou and W. Goldburg, Phys. Rev. A **20**, 2105 (1979).
[5] N. C. Wong and C. M. Knobler, Phys. Rev. A **24**, 3205 (1981).
[6] F. S. Bates and P. Wiltzius, J. Chem. Phys. **91**, 3258 (1989).
[7] M. Takenaka and T. Hashimoto, J. Chem. Phys. **96**, 6177 (1992).
[8] O. Mazurin and E. Porai-Koshits, *Phase Separation in Glass* (North-Holland, Amsterdam, 1984).
[9] A. J. Bray, Phil. Trans. R. Soc. A **361**, 781 (2003).
[10] A. J. Wagner and J. M. Yeomans, Phys. Rev. Lett. **80**, 1429 (1998).
[11] N. González-Segredo, M. Nekovee, and P. Coveney, Phys. Rev. E **67**, 046304 (2003).
[12] S. Ahmad, S. K. Das, and S. Puri, Phys. Rev. E **85**, 031140 (2012).
[13] H. Jinnai, Y. Nishikawa, H. Morimoto, T. Koga, and T. Hashimoto, Langmuir **16**, 4380 (2000).
[14] C. R. Lopez-Barron and C. W. Macosko, Langmuir **25**, 9392 (2009).
[15] D. G. Aarts, R. P. Dullens, and H. N. W. Lekkerkerker, New J. Phys. **7**, 40 (2005).
[16] A. Sicilia, J. Arenzon, A. J. Bray, and L. Cugliandolo, Phys. Rev. E **76**, 061116 (2007).
[17] A. Sicilia, Y. Sarrazin, J. Arenzon, A. J. Bray, and L. Cugliandolo, Phys. Rev. E **80**, 031121 (2009).
[18] S. Ahmad, F. Corberi, S. K. Das, E. Lippiello, S. Puri, and M. Zannetti, Phys. Rev. E **86**, 061129 (2012).
[19] S. Majumder and S. K. Das, Phys. Rev. Lett. **111**, 055503 (2013).
[20] H. Tanaka, J. Phys. Condens. Matter **12**, R207 (2000).
[21] V. Testard, L. Berthier, and W. Kob, J. Chem. Phys. **140**, 164502 (2014).
[22] K. Novik and P. Coveney, Phys. Rev. E **61**, 435 (2000).
[23] K. Luo, W. Gronski, and C. Friedrich, Macromol. Theory Simul. **13**, 365 (2004).
[24] J. Baruchel, J.-Y. Buffiere, P. Cloetens, M. Di Michiel, E. Ferrie, W. Ludwig, E. Maire, and L. Salvo, Scr. Mater. **55**, 41 (2006).
[25] J. Y. Buffiere, E. Maire, J. Adrien, J. P. Masse, and E. Boller, Exp. Mech. **50**, 289 (2010).
[26] A. Pyun, J. R. Bell, K. H. Won, B. M. Weon, S. K. Seol, J. H. Je, and C. W. Macosko, Macromolecules **40**, 2029 (2007).
[27] D. Dalmas, A. Lelarge, and D. Vandembroucq, J. Non-Cryst. Solids **353**, 4672 (2007).
[28] S. Schuller, O. Pinet, and B. Penelon, J. Am. Ceram. Soc. **94**, 447 (2011).
[29] A. Hodroj, P. Simon, P. Florian, M.-H. Chopinet, and Y. Vaills, J. Am. Ceram. Soc. **96**, 2454 (2013).
[30] E. M. Levin and G. M. Ugrinic, J. Res. Natl. Bur. Stand. **25**, 47 (1953).
[31] E. M. Levin and G. W. Cleek, J. Am. Ceram. Soc. **41**, 175 (1958).
[32] A. Chambolle, J. Math. Imaging Vision **20**, 89 (2004).
[33] L. Grady, IEEE Trans. Pattern Anal. Mach. Intell. **28**, 1768 (2006).
[34] Please see Supplemental Material at http://link.aps.org/supplemental/10.1103/PhysRevLett.112.245701 for details on the experimental setup, distributions of mean curvature, and a description of the sampling bias calculation for the size distribution of the domains.
[35] C. Lang, J. Ohser, and R. Hilfer, J. Microsc. **203**, 303 (2001).
[36] H.-J. Vogel, U. Weller, and S. Schlüter, Comput. Geosci. **36**, 1236 (2010).
[37] P. Sander and S. Zucker, IEEE Trans. Pattern Anal. Mach. Intell. **12**, 833 (1990).
[38] P. Ramachandran and G. Varoquaux, Comput. Sci. Eng. **13**, 40 (2011).
[39] E. D. Siggia, Phys. Rev. A **20**, 595 (1979).
[40] C. R. López-Barrón and C. W. Macosko, Soft Matter **6**, 2637 (2010).